

Optimal In-field Routing for Full and Partial Field Coverage with Arbitrary Non-Convex Fields and Multiple Obstacle Areas

Mogens Graf Plessen*

Abstract

Within the context of logistical optimisation in agriculture this paper discusses optimal in-field routing for full and partial field coverage with arbitrary non-convex fields and multiple obstacle areas. It is distinguished between 9 different in-field routing tasks: 2 for full field coverage, 7 for partial field coverage and 1 for shortest path planning between any 2 vertices of the transition graph. It is differentiated between equal or different start and end vertex for a task, coverage of only a subset of vertices, a subset of edges or combinations. Proposed methods are developed primarily for spraying and fertilising applications with larger operating widths and existence of a unique headland path. Partial field coverage where, e.g., only a specific subset of edges has to be covered is relevant for precision agriculture and also for optimised logistical operation of smaller-sized machinery with limited loading capacities. In this paper on the highest level it is distinguished between full and partial field coverage problems. For both modeling and solution algorithms are presented. Their characteristics are illustrated on 3 real-world fields.

Keywords: In-field Vehicle Routing; Full Field Coverage; Partial Field Coverage; Shortest Paths; Obstacle Areas.

1. Introduction and Problem Formulation

1.1. Motivation

Within the context of logistical optimisation in agriculture this paper is motivated by the desire to solve multiple in-field routing tasks differentiating, in particular, between full and partial field coverage, while simultaneously also accounting for non-convex fields, multiple obstacle areas, partitioned sub-fields, and compacted area minimisation. In general, it is thus aimed for optimisation of in-field coverage path planning, while generalising to different tasks and given field characteristics.

1.2. Problem Formulation and Contribution

The problem addressed is to write algorithms to solve the following 9 in-field routing tasks: (i) full field coverage with equal start and end vertex, (ii) full field coverage with different start and end vertex, (iii) coverage of a subset of vertices with equal start and end vertex, (iv) coverage of a subset of vertices with different start and end vertex, (v) coverage of a subset of edges with equal start and end vertex, (vi) coverage of a subset of edges with different start and end vertex, (vii) a combination of (iii) and (v), (viii) a combination of (iv) and (vi), and (ix) shortest path planning between any 2 vertices. As a starting point, the following assumptions are made: availability of a transition graph indicating all connections of vertices via edges, a corresponding cost array with edge-costs equal to the path length of edges, a designated start and end vertex, implementation of the task by 1 vehicle (instead of multiple in-field operating vehicles), and any of above (i)-(ix) in-field routing tasks.

For this setup, the contribution of this paper is to develop algorithms addressing the motivating aspects from Sect. 1.1.

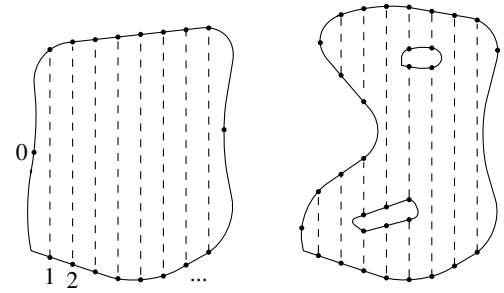


Fig. 1. Illustration of different types of field shapes and the notion of tractor traces defining a transition graph \mathcal{G} . Headland and interior edges are denoted by solid and dashed lines, respectively. Vertices are here indicated by dots and are, in general, labeled for identification such that the transition between any 2 vertices is unique. (Left) Uninterrupted edges when aligned in a rotated coordinate frame. (Right) Interrupted edges due to field indents and obstacle areas that are prohibited from trespassing by any vehicle operating in the field.

1.3. Background and Further Motivation

According to Ahumada & Villalobos (2009) there are four main functional areas for the agri-food supply chain: production, harvesting, storage and distribution. Logistical optimisation and route planning play an important role in all of the four functional areas for improved supply chain efficiency. Furthermore, according to Sørensen & Bochtis (2010) it can be distinguished between in-field, inter-field, inter-sector and inter-regional logistics. This paper relates to the first functional area of the agri-food supply chain, i.e., production, and further to in-field logistical optimisation.

The classic vehicle routing problem (VRP) seeks total cost-minimising routes for multiple identical vehicles that all start and end at a single depot and are subject to load constraints, and where multiple vertices (customers) subject to various demands must be serviced exactly once by exactly 1 vehicle. There are

*mgplessen@gmail.com

many variations, see Toth & Vigo (2014). The focus is on *vertex*-coverage. In contrast, for agricultural in-field routing typically *edge*-coverage is of primary importance. Often a single large machine is operating in-field, e.g., during a spraying application. Therefore, instead of VRPs, arc routing problems (ARPs) are here of more interest, see Eiselt et al. (1995a,b).

For shortest path planning between 2 vertices (routing task (ix) according to Sect. 1.2) greedy algorithms such as the algorithm by Dijkstra (1959) and the A*-algorithm by Hart et al. (1968) are famous. However, these are specialized algorithms that do not solve field coverage path planning problems where a set of edges needs to be covered. For ARPs according to Eiselt et al. (1995a,b), it can be distinguished between the classes of the Chinese postman problem (CPP) and the rural postman problem (RPP), where all and only a subset of all arcs of the graph need to be traversed, respectively. For the CPP it is further distinguished between undirected, directed, windy, mixed and hierarchical CPPs. Similarly, for RPPs. To further illustrate complexity of solution algorithms and their typical hierarchical structure, a directed RPP can be solved by first constructing a shortest spanning arborescence, then deriving an Eulerian graph on top, and ultimately determining an Eulerian tour on the augmented graph. In general, Eulerian tours on an Eulerian graph are not unique and can differ substantially. Therefore, specific heuristics can be derived to customise path planning behaviour.

Given an agricultural working area, the first step is to fit a transition graph with edges and vertices as their connection points. This step requires to (i) decide on field-interior edge shapes, straight or curved, and (ii) to account for field contours and possibly also for 3D topography, see Hameed et al. (2013a). According to Sect. 1.2, this paper assumes a transition graph given as starting point, whereby obstacle areas prohibited from trespassing are also accounted for according to Fig. 1.

See Griffel et al. (2018) and Seyyedhasani et al. (2019) for the role of field shapes on efficiency of path planning. In Zhou et al. (2014), a hierarchical and heuristic algorithm for in-field routing with obstacle areas is discussed. It is hierarchical since it decomposes the problem into 3 sequential stages. It is heuristic since it decomposes the field area first into cells, then determines a sequence for coverage of the cells, and only then considers path plans and their linking between the different cells. A similar method is described in Taïx et al. (2003). Importantly, because of these hierarchical heuristics and for transition graphs accounting for arbitrary field shapes and arbitrarily located multiple obstacles, these methods can in general not guarantee to find a minimum cost tour covering all edges at least once. This is mentioned to stress that, in contrast, the algorithm proposed in this paper is guaranteed to find the minimum cost tour. This is achieved by working directly on the full Eulerian graph augmentation. Heuristic rules are then derived on top to guide the planning of an Eulerian tour with favourable properties for additional partial field coverage and practical implementation.

Field decomposition into subfields using trapezoids as presented in Oksanen & Visala (2009) is a popular method to deal with irregularly shaped fields. See for instance also Mederle & Bernhardt (2017) and Santoro et al. (2017).

In Bochtis & Vougioukas (2008), Bochtis et al. (2013) and

MAIN NOMENCLATURE

\mathcal{E}	Set of all edges of \mathcal{G} : $(i, j) \in \mathcal{E}$.
\mathcal{E}'	Replicated edges added to \mathcal{G} to produce \mathcal{G}' .
$\mathcal{E}_{\text{hdl},\text{hdl}}^{\text{hdl}}$	Set of headland edges with vertices $i, j \in \mathcal{V}^{\text{hdl}}$.
$\mathcal{E}_{\text{isl},\text{isl}}^{\text{hdl}}$	Set of island headland edges with $i, j \in \mathcal{V}^{\text{isl}}$.
$\mathcal{E}_{\text{hdl},\text{isl}}^{\text{int}}$	Set of interior edges with $i \in \mathcal{V}^{\text{hdl}}, j \in \mathcal{V}^{\text{isl}}$.
$\mathcal{E}_{\text{isl},\text{isl}}^{\text{int}}$	Set of interior edges with $i \in \mathcal{V}^{\text{isl}}, j \in \mathcal{V}^{\text{isl}}$.
\mathcal{G}	Undirected transition graph, $\mathcal{G} = (\mathcal{V}, \mathcal{E})$.
\mathcal{G}'	Eulerian graph augmentation of \mathcal{G} .
\mathcal{I}	List of indices for partial field coverage.
$\mathcal{L}_{\mathcal{V}}$	Subset of vertices for partial field coverage.
$\mathcal{L}_{\mathcal{E}}$	Subset of edges for partial field coverage.
\mathcal{P}	Ordered list relevant for partial field coverage.
\mathcal{T}^{abu}	Tabu list of instances of \mathcal{I} , relevant in Alg. 2.
\mathcal{V}	Set of all vertices of \mathcal{G} .
\mathcal{V}^{hdl}	Set of headland vertices of \mathcal{G} .
\mathcal{V}^{isl}	Set of island vertices of \mathcal{G} .
C	Accumulated cost of a vertex-sequence, (m).
$N_{\mathcal{I}}, N_{\mathcal{T}^{\text{abu}}}$	2 scalar hyperparameters in Alg. 2.
$c_{i,j}$	Edge-cost (path length) for $(i, j) \in \mathcal{E}$, (m).
s_t	Vertex of a sequence $\{s_t\}_0^T$ at index t .
$\{s_t\}_0^T$	Sequence of vertices for $t = 0, \dots, T$.
$\{s_t^{\text{pfc}}\}_0^{T^{\text{pfc}}}$	Sequence of vertices for partial field coverage.
$\{s_t^{\text{sub}}\}_0^{T^{\text{sub}}}$	Subsequence of vertices for $t = 0, \dots, T^{\text{sub}}$.
$s_{\text{start}}, s_{\text{end}}$	Start and end vertex for a routing task.

Zhou et al. (2015), different fieldwork patterns and headland turning methods subject to vehicle kinematic constraints are discussed. They are typically motivated by the desire to minimise accumulated non-working path length at headlands. Note that these methods do not naturally account for in-field obstacles. Instead, as mentioned in the introduction of Bochtis et al. (2013), “*B-patterns do not generate any subfield areas division but, in contrast, the generation of the subfields (when it is needed due to e.g. physical obstacles or complex field shapes) is a prerequisite for applying B-patterns methodology*”. As a consequence, when accounting for obstacles (such as tree islands), B-patterns are in general no longer optimal since the same limitations of aforementioned hierarchical algorithms apply.

For the discussion of field experiments over 3 years for different headland turning methods see Paraforos et al. (2018).

Ultimately, in Plessen (2018) two path planning patterns for partial field coverage were compared for convex field shapes. One of them was identified as particularly favorable when aiming for minimal compacted area from tractor traces while accounting for limited turning radii of agricultural machinery. However, patterns are in general never optimal for arbitrary non-convex field shapes and when also considering multiple obstacle areas. In this perspective, the present paper is generalising and relevant not only for full but also for partial field coverage. Furthermore, as will be shown, algorithms are designed purposely such that the preferred pattern from Plessen (2018) is automatically recovered for convex field shapes.

The remaining paper is organised as follows. Algorithms are described in Sect. 2. Examples are provided in Sect. 3. Some more comments are in Sect. 4, before concluding with Sect. 5.

9 ROUTING TASKS

T1	Full field coverage with $s_{\text{start}} == s_{\text{end}}$.
T2	Full field coverage with $s_{\text{start}} \neq s_{\text{end}}$.
T3	Coverage of a subset of vertices with $s_{\text{start}} == s_{\text{end}}$.
T4	Coverage of a subset of vertices with $s_{\text{start}} \neq s_{\text{end}}$.
T5	Coverage of a subset of edges with $s_{\text{start}} == s_{\text{end}}$.
T6	Coverage of a subset of edges with $s_{\text{start}} \neq s_{\text{end}}$.
T7	A combination of T3 and T5.
T8	A combination of T4 and T6.
T9	Shortest path planning between any 2 vertices of \mathcal{G} .

Tab. 1. In this paper, 9 classes of in-field routing tasks are considered.

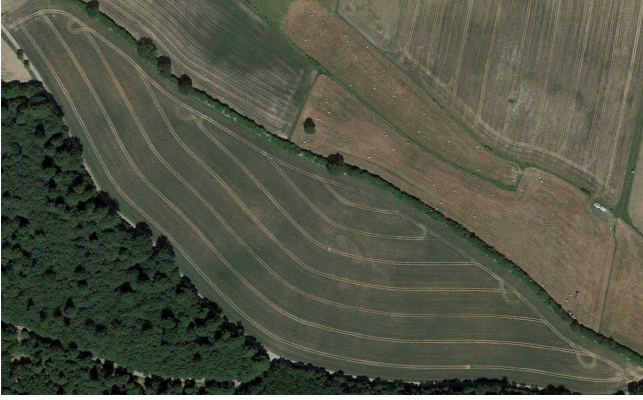


Fig. 2. Illustration of curved interior edges aligned to part of the field contour.

2. Solution Description

2.1. High-level strategy to address 9 different routing tasks

The 9 classes of different in-field routing tasks addressed in this paper are summarized in Tab. 1. In practice, this multitude is required for generality. For perspective, consider a spraying application occurring multiple times throughout any harvest year. Depending on available machinery, weather and varying available time-windows, different routing tasks apply, in particular, also for partial field coverage per field run. In view of precision agriculture, algorithmic solutions are therefore needed to address all of T1 to T9.

In this paper, it is distinguished between 2 main levels. On the highest level, there are the *full* field coverage tasks T1 and T2, whereby T2 can be considered as an extension of T1. The algorithm proposed therefore is discussed in Sect. 2.3. Then, on the second level, there are the *partial* field coverage tasks T3 to T8. Here, tasks T3, T5 and T7, and equivalently tasks T4, T6 and T8, exploit as their starting points the full field coverage solutions for T1 and T2, respectively. For the second level, the proposed algorithm is discussed in Sect. 2.4. Ultimately, T9 is a special case that is discussed in Sect. 2.5.

2.2. Preliminaries

Topographical characteristics relevant for in-field routing, data variables, and solution variables are discussed. For the

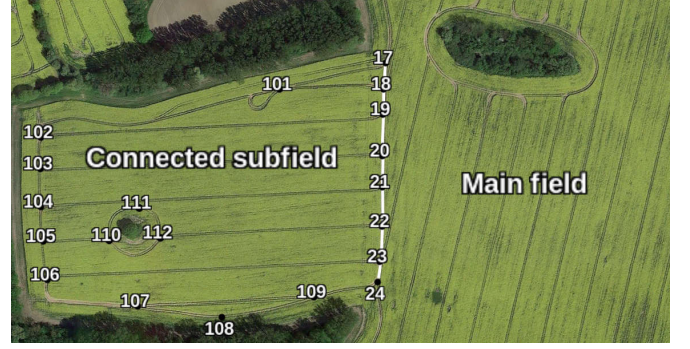


Fig. 3. Illustration of a subfield connected to the main field. Characteristic is (i) the sharing of a path, here from vertex 17 to 24, that is coinciding for both subfield and main field, and (ii) different interior edge orientations. The partition into main field and subfields occurs in particular in case of strongly non-convex fields, where it is worthwhile to differentiate interior edge orientations to minimise compacted area. The annotation is added for 2 reasons: (i) to illustrate vertex labeling on a satellite image, (ii) to emphasise that connected subfields and main field are treated separately according to Sect. 2.6.

former, these are (i) arbitrarily shaped fields (convex or non-convex), (ii) multiple obstacle areas¹ within the field, (iii) either straight or curved interior edges aligned to part of the field contour, and (iv) partitioned subfields with interior edges orientated differently from the area-wise largest main part of the field. See Fig. 2 and 3 for illustration. Two more comments are made. First, curved interior edges still permit a transition graph representation analogously to Fig. 1. Second, in this paper separate transition graphs are defined for all partitioned subfields and the main field. The synchronized handling of all of these is detailed in Sect. 2.6.

Data variables used for problem description are summarised in the main nomenclature table. See also Fig. 1 for visualisation. Some additional comments are made. First, for every undirected transition graph, $\mathcal{G} = (\mathcal{V}, \mathcal{E})$, the set of vertices and edges can be partitioned into subsets as follows:

$$\mathcal{V} = \mathcal{V}^{\text{hdl}} \cup \mathcal{V}^{\text{isl}}, \quad (1a)$$

$$\mathcal{E} = \mathcal{E}_{\text{hdl,hdl}}^{\text{hdl}} \cup \mathcal{E}_{\text{isl,isl}}^{\text{hdl}} \cup \mathcal{E}_{\text{hdl,isl}}^{\text{int}} \cup \mathcal{E}_{\text{isl,isl}}^{\text{int}}. \quad (1b)$$

Second, start and end vertex, s_{start} and s_{end} , typically denote the field entry and exit vertex. Third, a list of elements is denoted by $\{\cdot\}$, the number of elements in a list by $|\cdot|$, and an edge between vertices i and j by (i, j) . The “+”-operator is overloaded to indicate concatenation of lists as $\{\cdot\} + \{\cdot\}$. Fourth, throughout this paper, it is assumed that only *forward motion* of any in-field operating machinery is permitted. Thus, any sequence of vertices such as $a-b-a$ is prohibited since in practice for shortest path planning it would imply the necessity of reverse driving, which is impractical, in particular for operations with trailers and for large edge lengths. Fifth, as Fig. 1 illustrates, the number of edges incident to every vertex is either 2 or 3. However, because of the previous assumption about forward motion only, during routing at every vertex there are always only either 1 or

¹The term “obstacle area” comprises all obstacles prohibited from trespassing by in-field operating vehicles, including tree islands, ponds and so forth.

2 transition decisions possible. Ultimately, there always exists a path length minimising global optimal solution to all routing tasks T1 to T9. This immediately follows from the nonnegativity property of edge-costs, here defined as path lengths.

Solution variables most relevant in the presented algorithms are s_t , $\{s_t\}_0^T$, C , and variations with different superscripts. These indicate a vertex at index t , a sequence of vertices, and the accumulated path length, respectively.

2.3. Full Field Coverage: T1 and T2

Algorithm 1 is proposed for full field coverage path planning according to routing tasks T1 and T2.

Algorithm 1 Full Field Coverage for T1 and T2

0. **Required Subfunctions** (brief description):
 $\mathcal{F}^{\text{hdl}}(\cdot)$: for tracing of the headland path.
 $\mathcal{F}^{\text{fsp}}(\cdot)$: for the shortest path from s_{start} to s_{end} .
 $\mathcal{F}^{\text{sub}}(\cdot)$: for specific subtour computation.

1. **Data Input:** \mathcal{G}' , \mathcal{E}' , s_{start} and s_{end} .

2. $\{s_t\}_0^{T_{\text{hdl}}} \leftarrow \mathcal{F}^{\text{hdl}}(\mathcal{G}', s_{\text{start}}, s_{\text{start}})$.
3. $\{s_t\}_0^T \leftarrow \{s_t\}_0^{T_{\text{hdl}}} + \mathcal{F}^{\text{fsp}}(\mathcal{G}', s_{\text{start}}, s_{\text{end}})$.
4. $\mathcal{G}' \leftarrow \mathcal{G}' \setminus \{(s_t, s_{t+1})\}_0^{T_{\text{hdl}}-1}, \{(s_{t+1}, s_t)\}_0^{T_{\text{hdl}}-1}\}$, $\tau \leftarrow 0$.
5. **While** $\tau < |\{s_t\}_0^T| - 1$:
6. **If** $(s_\tau, s_{\tau+1}) \in \mathcal{E}'$:
7. $\{s_k^{\text{sub}}\}_{k=\tau+1}^{T_{\text{sub}}} \leftarrow \mathcal{F}^{\text{sub}}(s_{\tau+1}, s_\tau, \mathcal{G}')$.
8. $\mathcal{G}' \leftarrow \mathcal{G}' \setminus \{(s_\tau, s_{\tau+1}), (s_{\tau+1}, s_\tau)\}$.
9. $\{s_t\}_0^T \leftarrow \{s_t\}_0^T + \{s_k^{\text{sub}}\}_{k=\tau+1}^{T_{\text{sub}}} + \{s_k\}_{k=\tau+1}^T$.
10. $\mathcal{G}' \leftarrow \mathcal{G}' \setminus \{(\{s_k^{\text{sub}}, s_{k+1}^{\text{sub}}\})_{k=\tau+1}^{T_{\text{sub}}-1}, (\{s_{k+1}^{\text{sub}}, s_k^{\text{sub}}\})_{k=\tau+1}^{T_{\text{sub}}-1}\}$.
11. $\tau \leftarrow \tau + 1$.
12. $C \leftarrow \sum_{t=0}^{T-1} c_{s_t, s_{t+1}}$.

13. **Output:** $\{s_t\}_0^T$ and C .

Several explanatory comments are made. First, \mathcal{G}' denotes the Eulerian graph augmentation of the undirected graph \mathcal{G} . Thus, \mathcal{G} is augmented in a total minimum cost manner such that afterwards every vertex has even degree, i.e., an even number of incident edges, however, subject to the constraint that all interior edges shall not be eligible as augmentation candidates. The reason therefore is to enforce path planning with forward motion only for any in-field operating vehicle. Consequently, only headland edges and island headland edges are eligible. The edges replicated from \mathcal{G} for this augmentation are denoted by \mathcal{E}' . Due to the characteristic connectivity of \mathcal{G} with each vertex being connected to at most 3 vertices and aforementioned constraint, an Eulerian graph augmentation (see Bondy et al. (1976)) can always be constructed by pairing neighboring vertices in a cost-minimising manner. As a consequence, an overall path length minimising field coverage route for T1 with equal start end vertex is always constructed by traversing every edge at most twice. In contrast, for T2 with $s_{\text{start}} \neq s_{\text{end}}$, some

edges have to be traversed three times due to the final transition to s_{end} after completing the coverage of all edges of \mathcal{G} .

Second, function $\mathcal{F}^{\text{hdl}}(\cdot)$ returns $\{s_t\}_0^{T_{\text{hdl}}}$, which is the concatenation of the sequence of vertices tracing the headland path in counter clockwise (CCW) direction from s_{start} to s_{start} . The CCW direction is a choice, motivated by the desire to ultimately obtain consistent circular pattern-like path planning to be detailed below. Importantly, this choice does not compromise optimality since tracing complies with \mathcal{G}' and \mathcal{G}' is not affected thereby. Step 3 of Alg. 1, i.e., a shortest path computation on top of Step 2 only applies for T2 when s_{start} differs from s_{end} .

Third, in Step 4 all edges that were covered as part of Step 2 are removed from \mathcal{G}' in both directions, whereby they are removed only once. Thus, edges stemming from the Eulerian graph augmentation as well as all interior edges and island headland edges are unaffected and remain with \mathcal{G}' . Furthermore, edges that stem from the shortest path contribution due to T2 and Step 3 are not removed. The general consequence of Step 4 is a reduction of edge candidates from \mathcal{G}' available for future traversal in Steps 5-11.

Fourth, $\{s_t\}_0^T$ is traced throughout Steps 5-11. Then, as soon as an edge from the Eulerian graph augmentation is traversed in Step 6, a subtour is computed in Step 7 starting from vertex $s_{\tau+1}$ and ending at s_τ . The method for subtour computation is equivalent to a shortest path computation, however, here subject to 2 additional constraints plus 1 exploration heuristic. The 2 constraints are that (i) transitions along the headland path are feasible only in CCW-direction, and (ii) only forward motion and thus no $a-b-a$ sequence of vertices is permitted. The exploration heuristic is crucial. It enforces that as soon as an edge element of \mathcal{E}' is encountered throughout the path as a feasible next transition, then its exploration is enforced as the next transition. This exploration step is necessary to avoid making part of \mathcal{G}' disconnected at Step 10 of Alg. 1, in which case full field coverage would become impossible afterwards. Without the exploration heuristic and computation of just the shortest path between $s_{\tau+1}$ and s_τ , the possibility of disconnection occurs in particular in case of existence of multiple obstacle areas.

Fifth, Steps 8-10 of Alg. 1 are then responsible for removal of covered edges from \mathcal{G}' and insertion of the determined subtour in Step 7 into the main sequence of vertices, $\{s_t\}_0^T$, in Step 9. Note that the length of $\{s_t\}_0^T$ thus changes dynamically during runtime. Consequently, also the number of iterations according to Step 5 of Alg. 1 changes during runtime.

Sixth, in particular for convex field shapes and in the absence of obstacle areas, the enforcing of (i) traversal along all headland edges² only in CCW direction in combination with the enforcing of (ii) the traversal of all interior edges only once, and (iii) the corresponding Eulerian graph augmentation only along headland and island headland edges causes by design a particular circular path planning pattern visualised in Fig. 4. On the one hand, it is favorable for partial field coverage as discussed in Plessen (2018). However, it is also optimal when resulting

²Recall for emphasis that it is distinguished between headland edges and island headland edges according to Sect. 2.2. The CCW-direction constraint only holds for headland edges, but not for island headland edges.

from the application of Alg. 1. This follows directly from the fact that Alg. 1 works on the full Eulerian graph \mathcal{G}' , which ensures a minimum cost tour. The pattern is not optimal in particular in scenarios with multiple obstacle areas. However, then it naturally also does not occur in the solution of Step 13. Examples that illustrate this further are discussed in Sect. 3.

Seventh, any subtour, $\{s_k^{\text{sub}}\}_{\tau+1}^{\tau^{\text{sub}}}$, is inserted into the main sequence, $\{s_t\}_0^T$, at Step 9 of Alg. 1 immediately as soon as the subtour becomes available for traversal. As a consequence, interior edges are always covered first, before any continuation along the headland path until the next cover of interior edges according to a next inserted subtour. Furthermore, in case patterns according to Fig. 4 are determined from Step 7 for subtours, e.g., in the absence of obstacle areas and for convex fields, then for the concatenation of multiple of these patterns, interior edges are sequentially covered in *pairs*. This is favorable for the derivation of Alg. 2 for partial field coverage.

Ultimately, the output of Alg. 2 in Step 13 summarise the total accumulated cost (path length), C , computed in Step 12, and the corresponding sequence of vertices, $\{s_t\}_0^T$, of the path for full field coverage according to T1 and T2.

Algorithm 2 Partial Field Coverage for T3 to T8

0. **Required Subfunctions** (brief description):
 $\mathcal{F}^{\text{seq}}(\cdot)$: for sequential tracing of $\{s_t\}_0^T$.
 $\mathcal{F}^{\text{csp}}(\cdot)$: for concatenated shortest paths.
 $\mathcal{F}^{\text{r2n}}(\cdot)$: for randomly exchanging 2 neighbors.

0. **Hyperparameters**: $N_I, N_{\mathcal{T}^{\text{abu}}}$.

1. **Data Input**: $\mathcal{L}_V, \mathcal{L}_E, \mathcal{G}, \{s_t\}_0^T, s_{\text{start}}$ and s_{end} .

2. $\mathcal{P} \leftarrow \mathcal{F}^{\text{seq}}(\{s_t\}_0^T, \mathcal{L}_V, \mathcal{L}_E)$.
3. $I \leftarrow \{0, 1, \dots, |\mathcal{P}| - 1\}$.
4. $C^{\text{pfc}, \star}, \{s_t^{\text{pfc}, \star}\}_0^{T^{\text{pfc}, \star}} \leftarrow \mathcal{F}^{\text{csp}}(\mathcal{P}(I), \mathcal{G}, s_{\text{start}}, s_{\text{end}})$.
5. $\mathcal{T}^{\text{abu}} \leftarrow \{I\}, I^{\star} \leftarrow I, k \leftarrow 0$.
6. **While** $k < N_I$:
 7. $I \leftarrow \mathcal{F}^{\text{r2n}}(I^{\star}), j \leftarrow 0$.
 8. **While** $(I \in \mathcal{T}^{\text{abu}})$ **and** $(j < N_{\mathcal{T}^{\text{abu}}})$:
 9. $I \leftarrow \mathcal{F}^{\text{r2n}}(I)$, and $j \leftarrow j + 1$.
 10. **If** $I \notin \mathcal{T}^{\text{abu}}$:
 11. $\mathcal{T}^{\text{abu}} \leftarrow \{I\} + \mathcal{T}^{\text{abu}}(0 : \min(|\mathcal{T}^{\text{abu}}|, N_{\mathcal{T}^{\text{abu}}} - 1))$.
 12. $C^{\text{pfc}}, \{s_t^{\text{pfc}}\}_0^{T^{\text{pfc}}} \leftarrow \mathcal{F}^{\text{csp}}(\mathcal{P}(I), \mathcal{G}, s_{\text{start}}, s_{\text{end}})$.
 13. **If** $C^{\text{pfc}} < C^{\text{pfc}, \star}$:
 14. $C^{\text{pfc}, \star}, \{s_t^{\text{pfc}, \star}\}_0^{T^{\text{pfc}, \star}}, I^{\star} \leftarrow C^{\text{pfc}}, \{s_t^{\text{pfc}}\}_0^{T^{\text{pfc}}}, I$.
 15. $k \leftarrow k + 1$.

16. **Output**: $C^{\text{pfc}, \star}, \{s_t^{\text{pfc}, \star}\}_0^{T^{\text{pfc}, \star}}, I^{\star}$ and \mathcal{P} .

2.4. Partial Field Coverage: T3 to T8

Algorithm 2 is proposed for partial field coverage path planning according to routing tasks T3 to T8.

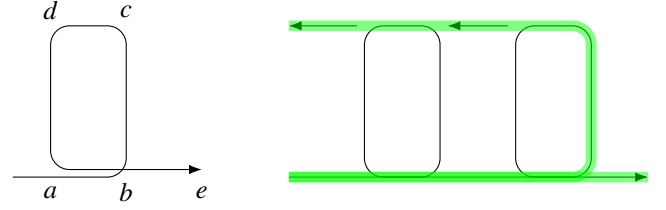


Fig. 4. (Left) Sketches of the field coverage pattern naturally resulting from the application of Alg. 1 for convex field shapes and in the absence of obstacle areas. The sequence of vertices, $\{a, b, c, d, e\}$, exemplarily illustrates the path planning for coverage of 2 straight edges (a, d) and (b, c) . (Right) Concatenation of 2 patterns and emphasis of 2 illustrative path transitions.

Several explanatory comments are made. First, \mathcal{L}_V and \mathcal{L}_E denote the lists of vertices and edges to be covered according to any respective task from T3 to T8. The coverage of specific vertices may be relevant, for example, for refilling of spraying tanks at a mobile depot waiting at a specified vertex at the field headland, or for the picking up or dropping off of, e.g., fertilising material. It is also included for generality.

Second, Step 2 of Alg. 2 is discussed. Function $\mathcal{F}^{\text{seq}}(\cdot)$ traces the output of T1 for T3, T5 and T7 or the output of T2 for T4, T6 and T8, before returning the list of edges *ordered* according to this tracing. Thus, this list can be written as $\mathcal{P} = \{\mathcal{P}_0, \mathcal{P}_1, \dots, \mathcal{P}_{|\mathcal{P}|-1}\}$, whereby each element

$$\mathcal{P}_i = (\{v_i^{\text{in}}\}, \{v_i^{\text{out}}\}), \quad \forall i = 0, \dots, |\mathcal{P}| - 1, \quad (2)$$

defines a directed edge with unique vertex v_i^{out} for both \mathcal{L}_V and \mathcal{L}_E , but unique v_i^{in} only for \mathcal{L}_E . Thus, $(v_i^{\text{in}}, v_i^{\text{out}}) \in \mathcal{L}_E$ and $v_i^{\text{out}} \in \mathcal{L}_V$. The notation $\{v_i^{\text{in}}\}$ in (2) is used since when tracing the tour $\{s_t\}_0^T$ in Step 2, there may be *multiple* vertices immediately *preceding* any $v_i^{\text{out}} \in \mathcal{L}_V$ throughout that tour. All of these vertices are stored in lists denoted by $\{v_i^{\text{in}}\}$, $\forall i = 0, \dots, |\mathcal{P}| - 1$. Thus, each list $\{v_i^{\text{in}}\}$ has length 1 for all $v_i^{\text{out}} \in \mathcal{L}_E$, but may have multiple entries for $v_i^{\text{out}} \in \mathcal{L}_V$ depending on the tour $\{s_t\}_0^T$.

Third, in Step 3 the initial ordering of \mathcal{P}_i -elements is determined and summarised in index-list I . In particular, for re-ordered instances of index-list I , the corresponding reordering of \mathcal{P}_i -elements shall be denoted by $\mathcal{P}(I)$.

Fourth, function $\mathcal{F}^{\text{csp}}(\cdot)$ returns a sequence of multiple concatenated shortest paths, $\{s_t^{\text{pfc}, \star}\}_0^{T^{\text{pfc}, \star}}$, and the corresponding accumulated cost, $C^{\text{pfc}, \star}$. Adding vertices, s_{start} and s_{end} , the following list can first be written,

$$\{s_{\text{start}}, \{v_{I_0}^{\text{in}}\}, v_{I_0}^{\text{out}}, \{v_{I_1}^{\text{in}}\}, v_{I_1}^{\text{out}}, \dots, \{v_{I_{|\mathcal{P}|-1}}^{\text{in}}\}, v_{I_{|\mathcal{P}|-1}}^{\text{out}}, s_{\text{end}}\}, \quad (3)$$

before *pairwise* shortest paths are computed, i.e., between pairs s_{start} and $\{v_{I_0}^{\text{in}}\}$, between $v_{I_0}^{\text{out}}$ and $\{v_{I_1}^{\text{in}}\}$, and so forth, until between $v_{I_{|\mathcal{P}|-1}}^{\text{out}}$ and s_{end} . For the case that any $\{v_{I_j}^{\text{in}}\}$ comprises more than 1 vertex, the shortest path between $v_{I_{j-1}}^{\text{out}}$ and *all* of their vertices is computed. The best vertex from $\{v_{I_j}^{\text{in}}\}$ is then selected such that the path length from $v_{I_{j-1}}^{\text{out}}$ to it *plus* the edge path length from it to $v_{I_j}^{\text{out}}$ is shortest. The return values, $\{s_t^{\text{pfc}, \star}\}_0^{T^{\text{pfc}, \star}}$ and $C^{\text{pfc}, \star}$, then represent the vertex sequence resulting from the concatenation of all pairwise shortest paths and the

corresponding accumulated path length, whereby any edges, $(\{v_{I_j}^{\text{in}}, v_{I_j}^{\text{out}}\})$, that link the different pairwise shortest paths are also included. The shortest path computation on \mathcal{G} is based on Dijkstra (1959), however, here accounting for 2 additional constraints: (i) transitions along the headland path are feasible only in CCW-direction in accordance with the method from Sect. 2.3 for full field coverage, (ii) directed edges $(v_{I_j}^{\text{out}}, \{v_{I_j}^{\text{in}}\})$, $\forall j = 0, \dots, |\mathcal{P}| - 1$ are prohibited from being on any corresponding shortest path between $v_{I_{j-1}}^{\text{out}}$ and $\{v_{I_j}^{\text{in}}\}$. The latter is done to enforce paths with forward motion only. Because of the special modeling technique with $(v_{I_j}^{\text{out}}, \{v_{I_j}^{\text{in}}\})$, $\forall j = 0, \dots, |\mathcal{P}| - 1$, plus the 2 vertices s_{start} and s_{end} , the length of (3) will always be even such that pairwise shortest path computations are always exactly possible.

Fifth, in Step 5 of Alg. 2, a *tabu list*, \mathcal{T}^{abu} , is initialised with indexing list \mathcal{I} . It is here also used to initialise the current best indexing list, \mathcal{I}^* , for the current best accumulated cost $C^{\text{pfc},*}$, before start of iterations from Step 6 on.

Sixth, the fundamental idea of Steps 6-15 is to iterate over indexing list \mathcal{I} with the purpose of improving cost $C^{\text{pfc},*}$ and the corresponding sequence of vertices, $\{s_t^{\text{pfc},*}\}_0^{T^{\text{pfc},*}}$. Function $\mathcal{F}^{\text{r2n}}(\cdot)$ in Steps 7 and 9 randomly exchanges 2 neighboring indices in \mathcal{I}^* and \mathcal{I} , respectively, to produce a new candidate list \mathcal{I} . It was found that in Step 7 attempting to exchange \mathcal{I}^* , instead of the last \mathcal{I} , improved performance. Similarly, it was found that incrementally exchanging only 2 neighboring indices yielded faster solve times vs. randomly reshuffling the entire \mathcal{I} -list at every iteration. Most importantly, it was found that the employment of a tabu list, \mathcal{T}^{abu} , significantly helped increasing the likelihood and speed of finding the global optimal $C^{\text{pfc},*}$. This is since the effect of \mathcal{T}^{abu} and Steps 8-10 is that exploration of different \mathcal{I} -candidates is enforced. According to Step 11, an \mathcal{I} not yet in \mathcal{T}^{abu} is added at index 0 and all remaining elements of \mathcal{T}^{abu} are shifted by 1 index, thereby deleting its previous last element if necessary to ensure a maximal length of the tabu list. More aspects of the size of \mathcal{T}^{abu} are discussed at the end of this section and in Sect. 4.

Seventh, the edges to be covered as a part of a routing task may be defined as *undirected* edges in $\mathcal{L}_{\mathcal{E}}$ when input to Alg. 2 as part of Step 1. However, after the tracing in Step 2, all edges of $\mathcal{L}_{\mathcal{E}}$ are automatically directed according to the transitions from $\{s_t\}_0^T$. Since the resulting \mathcal{P} is not changed beyond Step 2 in Alg. 2, also the direction of edge traversals is not further changed. This is done on purpose. In combination with the method of concatenating shortest paths subject to 2 constraints outlined above, it is thereby ensured that all transitions between any headland edge and any interior edge are unique. This in consequence is favourable w.r.t. minimisation of compacted area. If unique transitions were not enforced, then depending on a routing mission, an unconstrained shortest path computation may generate a *new* transition between a headland and interior edge, which in practice due to limited turning radii of in-field operating tractors would cause newly compacted area for this transition. Consequently, harvestable area would be destroyed and crop lost. Furthermore, in case there are many different partial field coverage missions, the consequence may even be that

at *every* transition from headland to interior and vice versa there are tractor traces in every which direction, which would be the worst-case scenario w.r.t. minimisation of compacted area.

Eighth, the motivation for the general methodology in Alg. 2 is underlined. In general, the partial field coverage problems can be considered as *traveling salesman problems* (TSPs) subject to additional constraints in the given setting. For general TSPs, the complexity scales extremely quickly. For n general entities to be visited, the number of different orders in which these can be visited is $n!$. For $n = 5$ this is $n! = 120$, however, for $n = 10$ it is already $n! = 3628800$. Key notion and the main argument for the design of Alg. 2 is that full field coverage can be considered as a special case for partial field coverage. For that particular case, the optimal solution is immediately recovered from Step 2-4 due to the fact that Alg. 2 starts for all partial field coverage solutions always initially from the full field coverage solutions for T1 and T2. In contrast, for alternative TSP-solution methods that would start from a more general setting, no guarantee may then be provided about the retrieval of the desired optimal full field coverage solution. Similarly, Alg. 2 is well suited for partial field coverage applications where groups of neighboring interior edges (pairs), or specific regions of the field are meant to be covered. This again follows from the initial tracing of the solution for full field coverage according to Step 2. Nevertheless, iteration steps 6-15 and in particular also the usage of the tabu list for exploration are still required for generality of partial field coverage missions, for example, when multiple distant apart vertices and edges need to be covered.

Ultimately, the 2 hyperparameters in Alg. 2, $N_{\mathcal{I}}$ and $N_{\mathcal{T}^{\text{abu}}}$, are discussed. An upper bound is $N_{\mathcal{T}^{\text{abu}}} \leq (|\mathcal{L}_{\mathcal{V}}| + |\mathcal{L}_{\mathcal{E}}|)!$. There is no gain from a larger tabu list since in that case \mathcal{T}^{abu} already can accomodate all possible sequences of vertices and edges of $\mathcal{L}_{\mathcal{V}}$ and $\mathcal{L}_{\mathcal{E}}$. Furthermore, it is sensible to bound $N_{\mathcal{I}} \geq N_{\mathcal{T}^{\text{abu}}}$ since the tabu list is otherwise never filled completely. For $N_{\mathcal{I}} > N_{\mathcal{T}^{\text{abu}}}$, there is a likelihood that throughout iteration Steps 6-15 the same \mathcal{I} is added multiple times to the tabu list, which does not yield exploration progress. Therefore, it is proposed

$$N_{\mathcal{I}} = N_{\mathcal{T}^{\text{abu}}}. \quad (4)$$

Then, there is only 1 hyperparameter in Alg. 2, which is also easy to tune: the larger the better for exploration and finding of the optimal solution. In practice, $N_{\mathcal{T}^{\text{abu}}}$ may be limited by a constrained or desired maximal solve time or above factorial bound for small problems. Examples are discussed in Sect. 3.2.

2.5. Special case: T9

The last in-field routing task for shortest path planning between any 2 vertices of \mathcal{G} may become relevant, for example, once a spraying tank is empty and it must be returned efficiently to a mobile depot waiting along the field boundary. The method for shortest path computation applied is identical to the one described in Sect. 2.4, where multiple shortest paths are concatenated. By non-negativity of edge weights and connectivity of \mathcal{G} there always exists a shortest path between any 2 vertices.

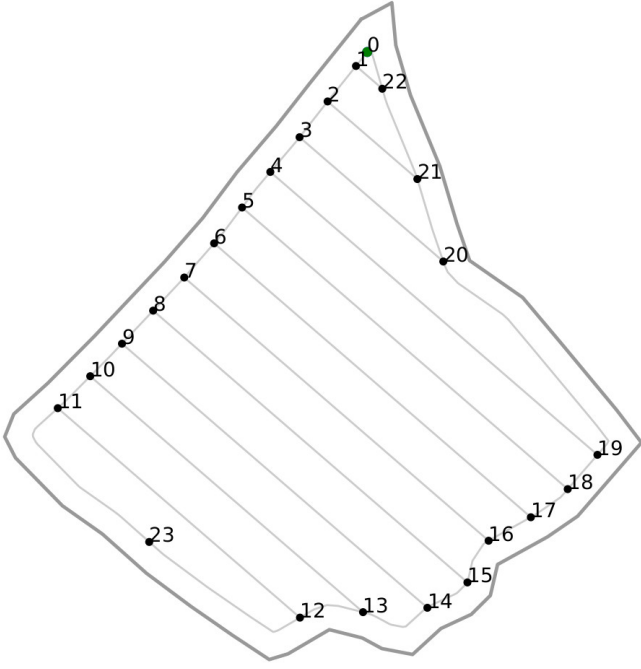


Fig. 5. Field 1. A real-world field of size 13.5ha. The operating width is 36m. The vertices of \mathcal{G} are labeled. The field entry and exit is vertex 0.

2.6. Special case: Handling of connected subfields

As mentioned in Sect. 2.2, *separate* transition graphs are defined for all partitioned subfields and the main field. Consequently, the algorithms for T1 and T2 from Sect. 2.3 for full field coverage, for T3 to T8 for partial field coverage, and T9 as a special case are all also applied *separately* to each of the subfields and the main field. However, for synchronisation 1 modification is implemented. While the headland traversal direction of the main field is defined as CCW, it is now defined as CW for all subfields. This is the only difference and permits to insert subfield solutions into the main field solution sequence of vertices, while ensuring consistent travel direction along the headland path segments coinciding for both the main and all connected subfields. For visualisation, see Fig. 3. According to above rules the travel sequence of vertices along the coinciding headland paths is $\{17, 18, \dots, 24\}$. An effect of this method to handle connected subfields is that part of the path coinciding for both main field and any subfield is covered 4 times.

3. Illustrative Examples

All methods are implemented in Python running an Intel i7-7700K CPU@4.2GHz×8 processor with 15.6 GiB memory.

3.1. Full Field Coverage Examples 1 to 3

Example 1 is based on the field in Fig. 5. There are no obstacle areas present. The optimal sequence of vertices, $\{s_i\}_0^T$, for full field coverage according to T1 is:

$$\{0, 1, 22, 0, 1, \mathbf{2, 3, 20, 21, 2, 3, 4, 5, 18, 19, 4, 5, 6, 7, 16, 17, 6, 7, 8, 9, 14, 15, 8, 9, 10, 11, 12, 13, 10, 11,}$$

$$23, 12, 13, 14, 15, 16, 17, 18, 19, 20, 21, 22, 0\}, \quad (5)$$

whereby the first occurrence of the pattern illustrated in Fig. 4, and which is naturally evolving from the application of Alg. 1, is emphasized in bold. Field size, number of vertices, path length and in particular computation times for Alg. 1 are summarized in Tab. 2. When tracing (5), there are 5 of aforementioned patterns concatenated for field coverage.

Example 2 is based on the field in Fig. 6. The optimal sequence of vertices, $\{s_i\}_0^T$, for full field coverage according to T2 with $s_{\text{start}} = 0$ and $s_{\text{end}} = 14$ is:

$$\{0, 1, 2, 63, 64, 65, 66, 1, 2, 3, 4, 61, 62, 3, 4, 5, 6, 59, \quad (6a)$$

$$60, 5, 6, 7, 8, 57, 58, 7, 8, 9, 10, 79, 98, \mathbf{97, 96, 55}, \quad (6b)$$

$$\mathbf{56, 97, 96, 95}, 94, 53, 54, 95, 94, 93, 92, 51, 52, 93, \quad (6c)$$

$$92, 91, 90, 49, 50, 91, 90, 89, 88, 47, 48, 89, 88, 87, \quad (6d)$$

$$86, 17, 18, 87, 86, 85, 84, 15, 16, 85, 84, 83, 82, 13, \quad (6e)$$

$$14, 83, 82, 81, 80, 11, 12, 81, 80, 79, 98, 9, 10, 11, \quad (6f)$$

$$12, 13, 14, 15, 16, 17, 18, 19, \mathbf{20, 75, 78, 77, 76, 45}, \quad (6g)$$

$$\mathbf{46, 77, 76, 75, 78, 19, 20, 21}, 22, 71, 74, 73, 72, 43, \quad (6h)$$

$$44, 73, 72, 71, 74, 21, 22, 23, 24, 41, 42, 23, 24, 25, \quad (6i)$$

$$26, 39, 40, 25, 26, 27, 28, 67, 70, 69, 68, 37, 38, 69, \quad (6j)$$

$$68, 67, 70, 27, 28, 29, 30, 35, 36, 29, 30, \mathbf{31, 32, 33}, \quad (6k)$$

$$\mathbf{34, 31, 32, 99}, 33, 34, 35, 36, 37, 38, 39, 40, 41, 42, \quad (6l)$$

$$43, 44, 45, 46, 47, 48, 49, 50, 51, 52, 53, 54, 55, 56, \quad (6m)$$

$$57, 58, 59, 60, 61, 62, 63, 64, 100, 65, 66, 0, 1, 2, 3, \quad (6n)$$

$$4, 5, 6, 7, 8, 9, 10, 11, 12, 13, 14\}, \quad (6o)$$

Several comments are made. First, in (6a) and (6b) multiple patterns can again be observed. Second, between (6b) and (6f) the coverage of the first and largest obstacle area with additional exploration of patterns outgoing from the island can be observed. The first pattern thereof is emphasised in bold in (6b) and (6c). The effect of exploration of interior edges connected to the island headland edges is an immediate result of the exploration heuristic discussed in Sect. 2.3. Third, in (6g)-(6h) the sequence of vertices for the covering of the second island is in bold for emphasis. Notably, the same method to cover the third and fourth island can be observed in (6h)-(6i), and also in (6j)-(6k), respectively. However, it cannot be deduced therefrom that islands with 4 interior edges incident are always handled optimally as indicated. Here, this is merely a coincidence due to the Eulerian graph augmentation for the particular field in Fig. 6. Nevertheless, from these cases deterministic consistency of the output from Alg. 1 can be observed, which is desirable. Fourth, in (6k)-(6l) the last pattern and coverage of the 2 last remaining interior edges is emphasised in bold. Afterwards, the sequence of vertices (6l)-(6o) proceeds along the headland for final coverage of not-yet covered headland edges. Because of the characteristic Eulerian graph augmentation and previous pattern-like coverage of interior edges, every second headland edge from vertex 34 up until 0 has not been covered to this point. Fifth and ultimately, (6o) results from the fact that s_{start} is different from s_{end} for this example.

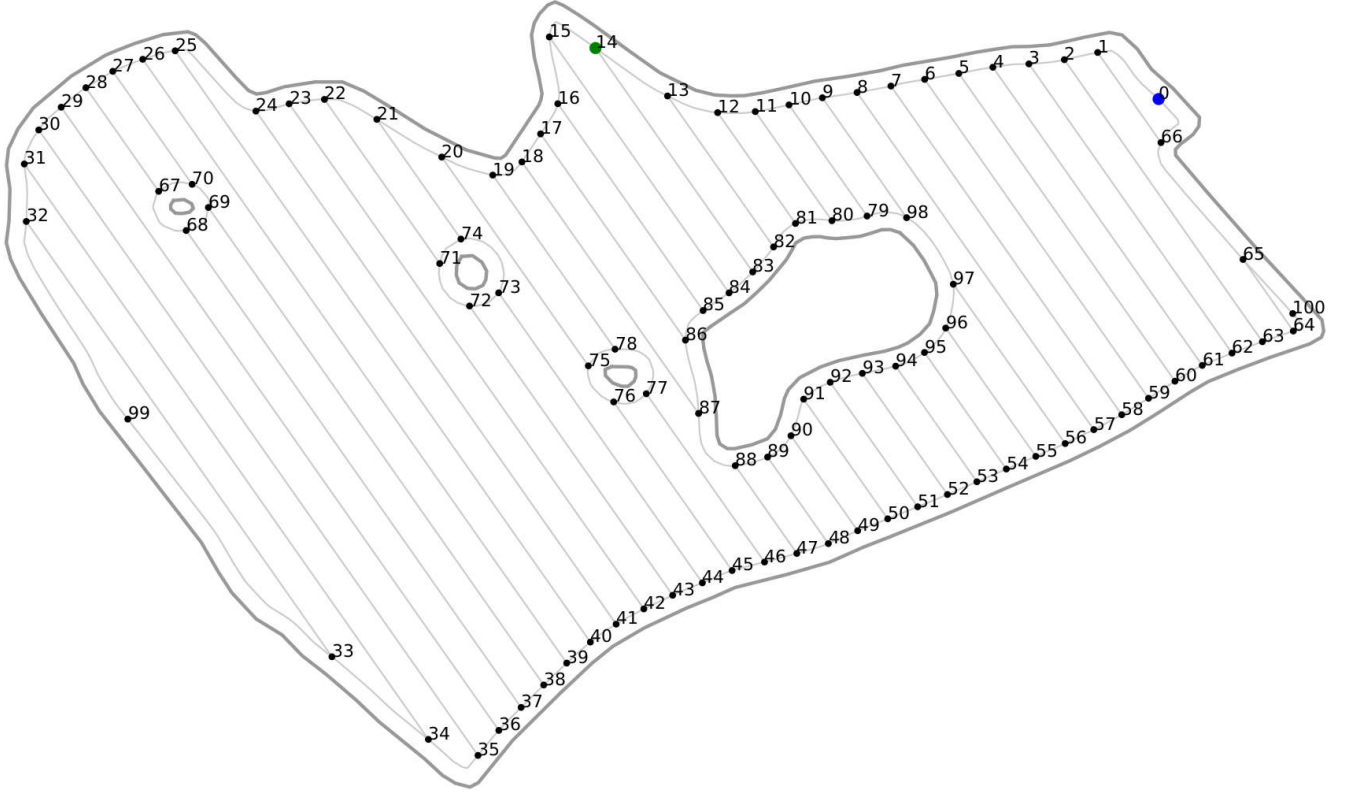


Fig. 6. Field 2. A real-world field of size 74.3ha. The operating width is 36m. There are 4 obstacle areas within field contours.

Example 3 is based on the field in Fig. 7. The optimal sequence of vertices, $\{s_i\}_0^T$, for field coverage according to T1 is:

$$\{0, 1, 2, 59, 60, 1, 2, 3, 4, 57, 58, 3, 4, 5, 6, 55, 56, 5, \quad (7a)$$

$$6, 7, 8, 53, 54, 7, 8, \mathbf{9, 10, 63, 64, 11, 12, 49, 50, 75, \quad (7b)$$

$$\mathbf{76, 77, 78, 61, 62, 63, 64, 61, 62, 77, 78, 75, 76, 51, \quad (7c)$$

$$\mathbf{52, 9, 10, 11, 12, 13, 14, 80, 81, 67, 66, 65, 70, 17, \quad (7d)$$

$$18, 43, 44, 65, 70, 69, 68, 15, 16, 69, 68, 67, 66, 45, \quad (7e)$$

$$46, 82, 79, 80, 81, 82, 79, 47, 48, 13, 14, 15, 16, 17, \quad (7f)$$

$$18, \mathbf{19, 20, 89, 88, 87, 86, 41, 42, 87, 86, 85, 84, 39, \quad (7g)$$

$$\mathbf{40, 85, 84, 83, 100, 37, 38, 83, 100, 99, 98, 35, 36, \quad (7h)$$

$$\mathbf{99, 98, 97, 96, 27, 28, 33, 34, 97, 96, 95, 94, 25, 26, \quad (7i)$$

$$\mathbf{95, 94, 93, 92, 23, 24, 93, 92, 91, 90, 71, 74, 73, 72, \quad (7j)$$

$$\mathbf{21, 22, 73, 72, 71, 74, 91, 90, 89, 88, 19, 20, 21, 22, \quad (7k)$$

$$23, 24, 25, 26, 27, 28, 29, 30, 31, 32, 29, 30, 101, 31, \quad (7l)$$

$$32, 33, 34, 35, 36, 37, 38, 39, 40, 41, 42, 43, 44, 45, \quad (7m)$$

$$46, 47, 48, 49, 50, 51, 52, 53, 54, 55, 56, 57, 58, 59, \quad (7n)$$

$$60, 0\}, \quad (7o)$$

Several comments are made. First, in (7a) multiple of aforementioned patterns can be observed. Second, the sequence of vertices covering both the first and second obstacle area is in bold for emphasis throughout (7b)-(7d). This sequence is not intuitive a priori. Edges are covered twice according to the Eu-

lerian graph augmentation. Third, the coverage of the third and fourth island is described in (7d)-(7f). Fourth, the sequence of vertices covering the fifth and sixth island is in bold for emphasis in (7g)-(7k). Similarly to Example 2, the exploration of interior edges connected to the headland island edges can be observed, which again is an immediate result of the exploration heuristic in Step 7 of Alg. 1.

3.2. Partial Field Coverage Examples 4 to 6

Three partial field coverage examples are discussed. The first is based on Fig. 5, while the latter 2 are based on Fig. 7.

For Example 4, the artificial problem setup comprises $\mathcal{L}_E = \{(6, 17), (9, 14), (20, 21)\}$. This in-field routing task classifies as T5, arguably the most relevant class for partial field coverage. For the results in Tab. 3, hyperparameters were set as $N_I = 6$ and $N_{T^{\text{abu}}} = 6$ since here $|\mathcal{L}_E| = 6$ and according to (4). The optimal sequence of vertices, $\{s_i^{\text{pfc},*}\}_0^T$, is:

$$\{0, 1, 2, 3, 4, 5, 6, 7, 8, \mathbf{9, 14, 15, 16, 17, 6, 7, 16,} \quad (8)$$

where all edges involving \mathcal{L}_E are in bold for emphasis. Two comments are made. First, note that edges from \mathcal{L}_E are initially undirected. However, as a consequence of Step 2 in Alg. 2, they become directed in the list of \mathcal{P} . These directions are then maintained throughout as emphasised in (8). Second, note how interior edge $(7, 16) \notin \mathcal{L}_E$ is traversed as part of the shortest path towards $(20, 21)$ after coverage of the 2 edges $(9, 14)$ and $(17, 6)$ that are element of \mathcal{L}_E .

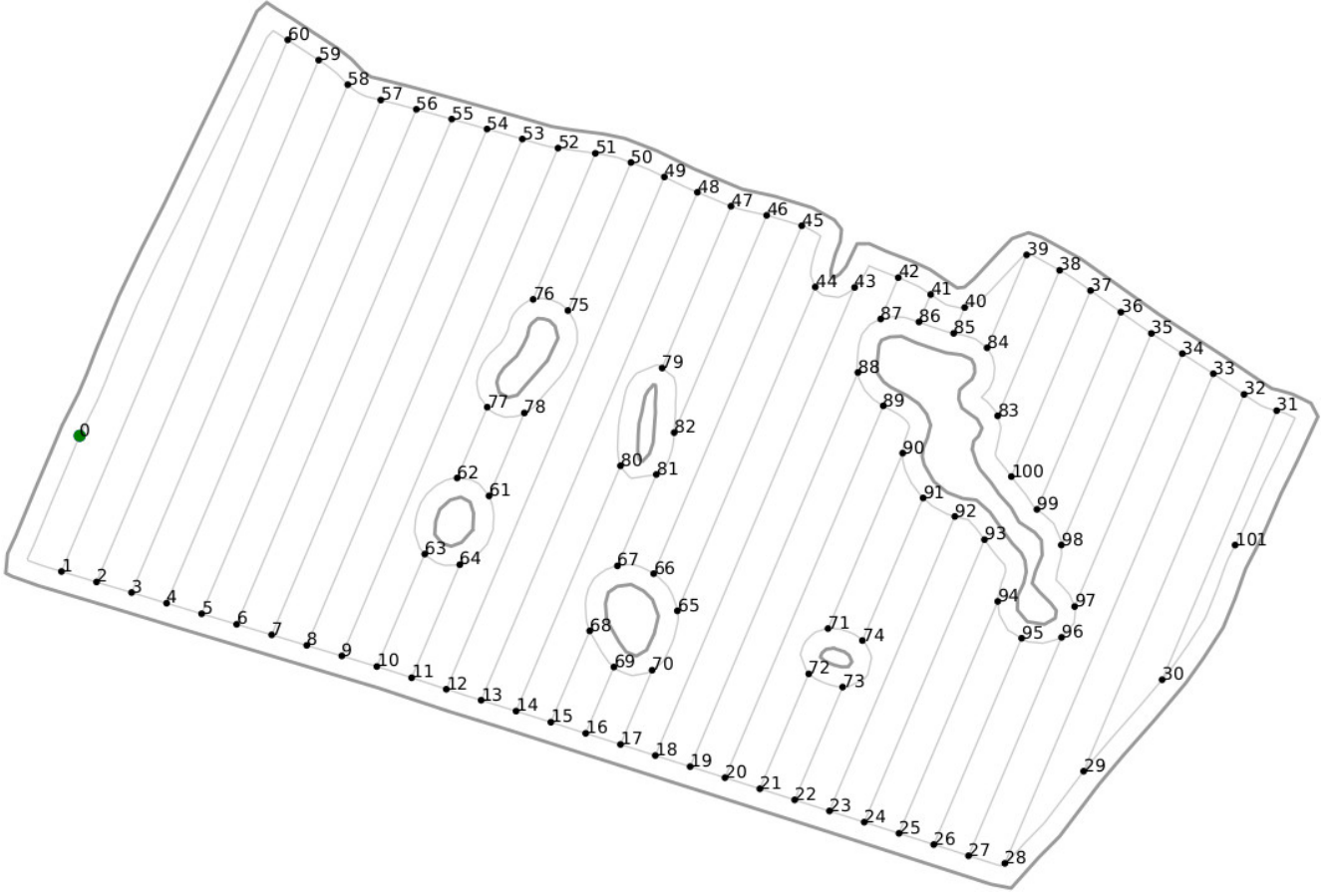


Fig. 7. Field 3. A real-world field of size 62.9ha. The operating width is 36m. There are 6 obstacle areas within field contours.

For Example 5, the artificial problem setup comprises 3 randomly and far apart selected vertices and edges, respectively. These are $\mathcal{L}_V = \{28, 91, 79\}$ and $\mathcal{L}_E = \{(63, 64), (54, 55), (101, 31)\}$. This in-field routing task thus classifies as T7. For the results in Tab. 3, hyperparameters were set as follows: $N_I = 50$ and $N_{T^{abu}} = 50$. The optimal sequence of vertices, $\{s_t^{pfs, \star}\}_0^{T^{pic, \star}}$, is:

$$\begin{aligned} &\{0, 1, 2, 3, 4, 5, 6, 7, 8, 9, 10, \mathbf{63, 64}, 11, 12, 13, 14, \\ &15, 16, 17, 18, 19, 20, 21, 22, 23, 24, 25, 26, \mathbf{27, 28}, \\ &29, 30, \mathbf{101, 31}, 32, 33, 34, 97, 96, 95, 94, 93, \mathbf{92, 91}, \\ &90, 89, 88, 87, 42, 43, 44, 45, 46, \mathbf{82, 79}, 47, 48, 49, \\ &50, 51, 52, 53, \mathbf{54, 55}, 56, 57, 58, 59, 60, 0\} \end{aligned} \quad (9)$$

where all edges involving \mathcal{L}_V and \mathcal{L}_E are in bold for emphasis. An additional comment is made. When tracing the output of T1, $\{s_t\}_0^T$, from (7) as part of Step 2 in Alg. 2, it is derived

$$\mathcal{P}_3 = \{(92, 74), 91\}. \quad (10)$$

This implies (i) that vertex 91, which is element of \mathcal{L}_V , is encountered at index $i = 3$, and further (ii) that this vertex has 2 candidate vertices, 92 and 74, immediately preceding vertex 91 in $\{s_t\}_0^T$ of T1. This possibility was discussed in detail in Sect. 2.4. As indicated in (9), the final optimal transition is (92, 91).

For Example 6, the problem setup comprises 8 edges to imitate a precision agriculture application where only specific edges, however, spread over the entire field, must be covered. These are $\mathcal{L}_E = \{(1, 60), (2, 59), (19, 88), (20, 89), (27, 96), (97, 34), (28, 33), (29, 32)\}$. For the results in Tab. 3, hyperparameters were set as follows: $N_I = 350$ and $N_{T^{abu}} = 350$. The optimal accumulated path length minimising sequence of vertices, $\{s_t^{pfs, \star}\}_0^{T^{pic, \star}}$, is:

$$\{0, 1, \mathbf{2, 59, 60, 1}, 2, 3, 4, 5, 6, 7, 8, 9, 10, 11, 12, 13, \quad (11a)$$

$$14, 15, 16, 17, 18, 19, \mathbf{20, 89, 88, 19}, 20, 21, 22, 23, \quad (11b)$$

$$24, 25, 26, 27, \mathbf{28, 33, 34, 97, 96, 27}, 28, 29, 30, 31, \quad (11c)$$

$$\mathbf{32, 29}, 30, 31, 32, 33, 34, 35, 36, 37, 38, 39, 40, 41, \quad (11d)$$

$$42, 43, 44, 45, 46, 47, 48, 49, 50, 51, 52, 53, 54, 55, \quad (11e)$$

$$56, 57, 58, 59, 60, 0\}, \quad (11f)$$

where all edges involving \mathcal{L}_E are in bold for emphasis. Two comments are made. First, in this example the second constraint discussed in Sect. 2.4 for the specific shortest path computation to enforce forward motion only becomes active. The result is the sequence of vertices in (11c), $\{28, 29, 30, 31\}$, preceding the directed edge traversal (32, 29) in (11d). Second, notice how interior edge (30, 31) is covered *twice* throughout (11). The second traversal in (11d) is part of the shortest path back to $s_{\text{end}} = 0$, after coverage of the last remaining edge from \mathcal{L}_E .

Ex.	Size	$ \mathcal{V} $	Path length	T_{solve}
1	13.5ha	24	4624.5m	0.0002s
2	74.3ha	101	26026.7m	0.0015s
3	62.9ha	102	21974.3m	0.0016s

Tab. 2. Full field coverage examples. Summary of results. Examples 1-3 correspond to Fields 1-3 in Fig. 5-7. Computation runtimes for Alg. 1 are in bold for emphasis.

Ex.	Path length	T_{solve}
4	1924.5m	0.0012s
5	4482.9m	0.1644s
6	7413.4m	1.3984s

Tab. 3. Partial field coverage examples. Summary of results. Example 4 refers to Field 1, while Example 5 and 6 correspond to Field 3. Computation runtimes for Alg. 2 are in bold for emphasis. Hyperparameter choices used for the 3 examples are $(N_{\mathcal{I}}, N_{\mathcal{T}^{\text{abu}}}) = (6, 6)$, $(50, 50)$ and $(350, 350)$, respectively.

For full field coverage, all interior edges were constrained to be covered only once as part of the Eulerian graph augmentation in order to ensure forward motion and to encourage circular pattern-like optimal path planning whenever applicable. However, for partial field coverage, this constraint is dropped to minimise path length and soil strain due to tractor traces. Importantly, all transitions between interior edges and headlands are still fully compatible with the results for full field coverage, such that no new compacted areas due to limited turning radii of in-field operating vehicles are created.

Finally, hyperparameter choices and the role of the tabu list are discussed. It was observed that the inclusion of a tabu list, \mathcal{T}^{abu} , in Alg. 2 significantly helped to retrieve the global optimal solution for partial field coverage tasks. Furthermore, by increasing the size of the tabu list, exploration is more enforced and the process of finding the optimum is significantly accelerated. For example, when reducing the maximal tabu list size to $N_{\mathcal{T}^{\text{abu}}} = 25$ for both Examples 5 and 6, and to still retrieve the optimal solution, $N_{\mathcal{I}}$ had to be increased to 100 and 650, respectively. Then, the corresponding solve times for these scenarios were 0.3306s and 2.7173s, which are roughly twice as large as the results in Tab. 3. To stress this more, when reducing $N_{\mathcal{T}^{\text{abu}}}$ to 10 in Example 6, it had to be set $N_{\mathcal{I}} = 3300$ before recovering the optimal solution, which resulted in $T_{\text{solve}} = 14\text{s}$. To summarize, it was found that inclusion of the tabu list in Alg. 2 is a simple but very effective method to enforce exploration and speed up solve times. The larger the tabu list the better the exploration throughout Alg. 2.

4. More Comments and Discussion of Limitations

One benefit of proposed methods are very small computation times for T_{solve} . As Tab. 2 demonstrates, this holds in particular for full field coverage tasks T1 and T2 and is a consequence from starting with an Eulerian graph \mathcal{G}' before subsequently removing covered edges such that the set of feasible edge transitions shrinks with iterations, which further accelerates runtimes. In contrast, as Tab. 3 demonstrates for partial field cov-

erage applications, T_{solve} is typically higher. Similarly to traveling salesman problems, here additionally with constraints enforcing forward motion and traversal along the headland only in CCW-direction, the sequence in which to trace a subset of vertices or edges is not straightforward to compute, in particular if multiple obstacle areas are present.

Another benefit of proposed methods are the total absence of hyperparameters in Alg. 1 and the presence of only 2 hyperparameters in Alg. 2. Preferably, also just 1 according to (4). As pointed out towards the end of Sect. 3.2, the larger the maximal tabu list size, $N_{\mathcal{T}^{\text{abu}}}$, the better for enforcing exploration. For a very small number of vertices and edges to cover, one can select $N_{\mathcal{T}^{\text{abu}}} = (|\mathcal{L}_{\mathcal{E}}| + |\mathcal{L}_{\mathcal{V}}|)!$, which guarantees that all possible sequences of vertices and edges to cover will be tested.

The main practical limitation of proposed methods is unintuitive path planning, in particular in presence of multiple obstacle areas. One may argue that even if the returned sequence of vertices is path length optimal, it may still be not implementable. As long as tractors are not fully automatically tracking path plans, e.g., similarly to the method from Plessen & Bemporad (2017), fully optimised path plans may not be practical. This is since the vehicle driver has to be “glued to” a navigation screen and audio commands to follow an unintuitive path plan while simultaneously concentrating on keeping track, which may be stressful to the driver. However, it is emphasised that this aspect is explicitly addressed and mitigated by the design of Alg. 1 and 2 through the enforcement of pattern-like field coverage whenever applicable, which (i) then maintains optimality since being based on \mathcal{G}' , and which (ii) can favorably be translated to consistent rule-based driving instructions at least for all convex fields, such that (iii) unintuitive paths remain only for field portions with multiple obstacle areas.

5. Conclusion

This paper discussed optimal in-field routing for full and partial field coverage with arbitrary non-convex fields and multiple obstacle areas. It is distinguished between 9 different in-field routing tasks: 2 for full field coverage, 7 for partial field coverage and 1 for shortest path planning between any 2 vertices of the transition graph. It is differentiated between equal and different start and end vertex for a task, coverage of all edges (full field coverage), or coverage of only a subset of vertices, a subset of edges or combinations (partial field coverage). Key notion is how to efficiently combine coverage of headland and island headland edges together in combination with coverage of all interior edges. Starting from an Eulerian graph augmentation, proposed algorithms encourage a particular circular-like pattern whenever applicable without compromising optimality, such that field coverage is consistent for convexly shaped fields. For arbitrary non-convex fields and with multiple obstacle areas, resulting path guidance is not intuitive anymore, however, path length optimal. Proposed methods are primarily developed for spraying and fertilising applications with larger working widths of corresponding in-field operating vehicles. The handling of subfields connected to the main field was discussed. The proposed solution for partial field coverage starts from the

solution for full field coverage to consistently comply with transitions between interior and headland edges by accounting for limited turning radii of agricultural vehicles, and thereby ensuring that no new tractor traces are generated in view of compacted area minimisation. For partial field coverage, the benefit of employing a tabu list in the solution algorithm for improved exploration was highlighted. Proposed methods were illustrated by means of 6 experiments on 3 real-world fields, with a focus on demonstrating small computation runtimes and the explicit mentioning of sequences of vertices to emphasise aspects of presented path planning methods.

References

- Ahumada, O., & Villalobos, J. R. (2009). Application of planning models in the agri-food supply chain: A review. *European Journal of Operational Research*, 196, 1–20.
- Bochtis, D., Griepentrog, H. W., Vougioukas, S., Busato, P., Berruto, R., & Zhou, K. (2015). Route planning for orchard operations. *Computers and electronics in agriculture*, 113, 51–60.
- Bochtis, D., & Vougioukas, S. (2008). Minimising the non-working distance travelled by machines operating in a headland field pattern. *Biosystems engineering*, 101, 1–12.
- Bochtis, D. D., Sørensen, C. G., Busato, P., & Berruto, R. (2013). Benefits from optimal route planning based on B-patterns. *Biosystems engineering*, 115, 389–395.
- Bondy, J. A., Murty, U. S. R. et al. (1976). *Graph theory with applications* volume 290. Citeseer.
- Dijkstra, E. W. (1959). A note on two problems in connexion with graphs. *Numerische mathematik*, 1, 269–271.
- Eiselt, H. A., Gendreau, M., & Laporte, G. (1995a). Arc routing problems, part i: The chinese postman problem. *Operations Research*, 43, 231–242.
- Eiselt, H. A., Gendreau, M., & Laporte, G. (1995b). Arc routing problems, part ii: The rural postman problem. *Operations research*, 43, 399–414.
- Griffel, M. L., Vazhnik, V., Hartley, D., Hansen, J. K., & Richard, T. L. (2018). Machinery maneuvering efficiency and perennial crops: field shape complexity defines the efficiency. In *2018 ASABE Annual International Meeting* (p. 1). American Society of Agricultural and Biological Engineers.
- Hameed, I., Bochtis, D., Sørensen, C. G., Jensen, A. L., & Larsen, R. (2013a). Optimized driving direction based on a three-dimensional field representation. *Computers and electronics in agriculture*, 91, 145–153.
- Hameed, I. A., Bochtis, D., & Sørensen, C. (2011). Driving angle and track sequence optimization for operational path planning using genetic algorithms. *Applied Engineering in Agriculture*, 27, 1077–1086.
- Hameed, I. A., Bochtis, D., & Sørensen, C. A. (2013b). An optimized field coverage planning approach for navigation of agricultural robots in fields involving obstacle areas. *International journal of advanced robotic systems*, 10, 231.
- Hart, P. E., Nilsson, N. J., & Raphael, B. (1968). A formal basis for the heuristic determination of minimum cost paths. *IEEE transactions on Systems Science and Cybernetics*, 4, 100–107.
- Jensen, M. A. F., Bochtis, D., Sørensen, C. G., Blas, M. R., & Lykkegaard, K. L. (2012). In-field and inter-field path planning for agricultural transport units. *Computers & Industrial Engineering*, 63, 1054–1061.
- Mederle, M., & Bernhardt, H. (2017). Analysis of influencing factors and decision criteria on infield-logistics of different farm types in germany. *Agricultural Engineering International: CIGR Journal*, 19, 139–148.
- Oksanen, T., & Visala, A. (2009). Coverage path planning algorithms for agricultural field machines. *Journal of Field Robotics*, 26, 651–668.
- Paraforos, D. S., Hübner, R., & Griepentrog, H. W. (2018). Automatic determination of headland turning from auto-steering position data for minimising the infield non-working time. *Computers and electronics in agriculture*, 152, 393–400.
- Plessen, M. M. G. (2018). Partial field coverage based on two path planning patterns. *Biosystems engineering*, 171, 16–29.
- Plessen, M. M. G., & Bemporad, A. (2017). Reference trajectory planning under constraints and path tracking using linear time-varying model predictive control for agricultural machines. *Biosystems engineering*, 153, 28–41.
- Rodias, E., Berruto, R., Busato, P., Bochtis, D., Sørensen, C., & Zhou, K. (2017). Energy savings from optimised in-field route planning for agricultural machinery. *Sustainability*, 9, 1956.
- Santoro, E., Soler, E. M., & Cherri, A. C. (2017). Route optimization in mechanized sugarcane harvesting. *Computers and Electronics in Agriculture*, 141, 140–146.
- Seyyedhasani, H., Dvorak, J. S., & Roemmele, E. (2019). Routing algorithm selection for field coverage planning based on field shape and fleet size. *Computers and Electronics in Agriculture*, 156, 523–529.
- Sørensen, C. G., & Bochtis, D. D. (2010). Conceptual model of fleet management in agriculture. *Biosystems Engineering*, 105, 41–50.
- Taix, M., Souères, P., Frayssinet, H., & Cordesses, L. (2003). Path planning for complete coverage with agricultural machines. In *Field and service robotics* (pp. 549–558). Springer.
- Toth, P., & Vigo, D. (2014). *Vehicle routing: problems, methods, and applications*. SIAM.
- Yu, X., Roppel, T. A., & Hung, J. Y. (2015). An optimization approach for planning robotic field coverage. In *IECON 2015-41st Annual Conference of the IEEE Industrial Electronics Society* (pp. 004032–004039). IEEE.
- Zhou, K., Jensen, A. L., Bochtis, D. D., & Sørensen, C. G. (2015). Quantifying the benefits of alternative fieldwork patterns in a potato cultivation system. *Computers and Electronics in Agriculture*, 119, 228–240.
- Zhou, K., Jensen, A. L., Sørensen, C. G., Busato, P., & Bochtis, D. (2014). Agricultural operations planning in fields with multiple obstacle areas. *Computers and electronics in agriculture*, 109, 12–22.